AC

MAD-PH 816

Su 3413

University of Wisconsin - Madison

MAD/PH/816
January 1994

The Asymmetric Flux Tube

M. G. Olsson and Siniša Veseli

Department of Physics, University of Wisconsin, Madison, WI 53706

Abstract

We consider a relativistic flux tube with arbitrary mass spinless quarks at the ends. A classical circular solution is found. The quantized equations corresponding to mesons at rest are constructed and solved. A comparison is made with all available spin-averaged heavy-light and heavy-heavy states.

1 Introduction

The relativistic flux tube (RFT) model shows promise to provide a realistic description of all meson states. The RFT model is in essence a description of dynamical confinement [1]-[4]. For slowly moving quarks rigorous QCD relativistic corrections [5]-[7] clearly demonstrate that the scalar confinement potential picture is incorrect [2, 7]. On the other hand, the RFT dynamics are consistent with both spin-dependent [3, 8, 9] and spin-independent [2, 3] QCD expectations. The basic assumption of the RFT model is that the QCD dynamical ground state for large quark separation consists of a rigid straight tubelike color flux configuration connecting the quarks. In this idealized limit the quarks and tube are shown in Fig. 1.

The heavy-light mesons are important for many reasons. For our present purposes, these mesons exhibit relativistic dynamics while still maintaining some simplifying aspects. The heavy quark mass supresses most spin dependence so that a spinless quark analysis has considerable validity. The one heavy quark also means the reduced Salpeter equation [10] will be appropriate and that relative time degrees of freedom are unimportant.

Although a full RFT analysis of heavy-light mesons with fermionic quarks has not yet been completed, our present spinless calculation is useful for several reasons:

1. The extension to unequal quark masses requires the solution of several technical problems. These problems have their origin in locating the center of momentum and ensuring that the total momentum of the meson vanishes.

2. Both spinless and fermionic quark analyses share a common orbital angular momentum analysis. The techniques developed here will therefore be of direct utility in the more realistic calculation.

3. Because of the suppressed spin dependence due to the small color magnetic moment of the heavy quark, a spin-averaged analysis is realistic.

4. We reconsider the question of the symmetrization of operators in the quantized RFT equations. Algorithms are developed for finding the symmetrical perpendicular velocity operators.

As established previously [1]-[4] the classical angular momentum of two quarks plus two tube segments joined at the CM is

$$J = W_{r_1}\gamma_{\perp_1}v_{\perp_1}r_1 + 2ar_1^2 f(v_{\perp_1}) + (1 \to 2) \ , \tag{1}$$

where

$$W_{r_i} = \sqrt{p_{r_i}^2 + m_i^2} \ , \tag{2}$$

$$4v_\perp f(v_\perp) = \frac{\arcsin v_\perp}{v_\perp} - \gamma_\perp^{-1} \ , \tag{3}$$

$$\gamma_\perp^{-2} = 1 - v_\perp^2 \ . \tag{4}$$

The classical hamiltonian for this system is

$$H = W_{r_1}\gamma_{\perp_1} + ar_1\frac{\arcsin v_{\perp_1}}{v_{\perp_1}} + (1 \to 2) \ . \tag{5}$$

For unequal mass quarks additional conditions [3] must be imposed so that the meson CM is at rest

$$p_{r_1} = p_{r_2} \equiv p_r \ , \tag{6}$$

$$P_\perp = 0 = W_{r_1}\gamma_{\perp_1}v_{\perp_1} + a\frac{r_1}{v_{\perp_1}}(1 - \gamma_{\perp_1}^{-1}) - (1 \to 2) \ . \tag{7}$$

Finally, the straight flux tube condition is

$$\frac{v_{\perp_1}}{r_1} = \frac{v_{\perp_2}}{r_2} \ . \tag{8}$$

For equal mass quarks the $P_\perp$ condition (7) is satisfied since $v_{\perp_1} = v_{\perp_2}$. For $m_2 \gg m_1$ and also $m_2 \gg ar_1$ the $P_\perp$ condition can be satisfied with $v_{\perp_2} \simeq 0$ (i.e., the CM point is coincident with the heavy quark). For all other (asymmetrical)

mesons all of the above relations (1-7) must be used in the construction of the solution.

In section 2 we consider the purely rotational classical solutions to the RFT equations. These results will provide useful correspondence check on the quantum solution. Section 3 formulates the quantized RFT equations and their solutions are discussed in section 4. In section 5 we test the model by comparing to all observed spin-averaged masses of mesons containing one or two heavy quarks. Our conclusions are summarized in section 6.

2 Classical (Yrast) Solution

The classical solution of the RFT equations having minimum energy for a given angular momentum (the *yrast* solution corresponds to circular motion, i.e., $p_r = 0$). In this case the RFT equations (1) and (5) become

$$J = m_1\gamma_{\perp_1}v_{\perp_1}r_1 + 2ar_1^2 f(v_{\perp_1}) + (1 \to 2) \ , \tag{9}$$

$$H = m_1\gamma_{\perp_1} + ar_1\frac{\arcsin v_{\perp_1}}{v_{\perp_1}} + (1 \to 2) \ . \tag{10}$$

The condition (7) that the CM momentum vanishes becomes

$$P_\perp = 0 = m_1\gamma_{\perp_1}v_{\perp_1} + a\frac{r_1}{v_{\perp_1}}(1 - \gamma_{\perp_1}^{-1}) - (1 \to 2) \ . \tag{11}$$

Along with the straight tube condition (8), the above three relations can be used to find the yrast solution $M = H(J)$.

A short cut to the yrast solution directly uses the circular dynamical condition. In the lagrangian approach [1, 11] the radial derivative of the lagrangian, must vanish since $\dot{p}_r = 0$. Another way to obtain the same result is to consider the force on the i^{th} quark in two reference systems. In its rest frame the quark experiences a force $-a\hat{\mathbf{r}}_i$ due to the tube. In the CM rest frame, where the quark is moving with the

velocity $v_\perp$ perpendicular to the tube, the transverse force is $a/\gamma_{\perp_i}$ and for circular orbite this must equal the mass $m_i\gamma_{\perp_i}$ times the centripetal acceleration or

$$(m_i\gamma_{\perp i})\frac{v_{\perp_i}^2}{r_i} = \frac{a}{\gamma_{\perp_i}} \ . \tag{12}$$

This, along with the straight string condition (8), assures that the meson is at rest (i.e., the total linear momentum (11) vanishes). From (12) we also have

$$v_{\perp_i}^2 = \frac{ar_i}{m_i + ar_i} \ , \tag{13}$$

$$\gamma_{\perp_i}^2 = 1 + \frac{ar_i}{m_i} \ . \tag{14}$$

The total interquark distance is evidently

$$r = r_1 + r_2 \ , \tag{15}$$

and using (8) and (13), we obtain

$$r_1 = \frac{m_2 + ar}{m_1 + m_2 + 2ar} \ . \tag{16}$$

$$r_2 = \frac{m_1 + ar}{m_1 + m_2 + 2ar} \ . \tag{17}$$

When the above expressions are substitued back into (13) and (14), we find

$$v_{\perp_1}^2 = \frac{ar(m_2 + ar)}{(m_1 + ar)(m_1 + m_2 + ar)} \ , \tag{18}$$

$$v_{\perp_2}^2 = \frac{ar(m_1 + ar)}{(m_2 + ar)(m_1 + m_2 + ar)} \ , \tag{19}$$

$$\gamma_{\perp_i}^2 = \frac{(m_i + ar)(m_1 + m_2 + ar)}{m_i(m_1 + m_2 + 2ar)} \ . \tag{20}$$

The quantities $r_i, v_{\perp_i}$ and $\gamma_{\perp_i}$ have now been expressed in terms of the interquark distance r. The circular RFT equations can similarly be expressed in terms of r. Equation (9) for the meson angular momentum becomes

$$2\frac{J}{r} = \frac{\sqrt{ar}}{(m_1 + m_2 + 2ar)^{\frac{3}{2}}}\left[\sqrt{m_1}(m_2 + ar)^{\frac{3}{2}} + \sqrt{m_2}(m_1 + ar)^{\frac{3}{2}}\right]$$
$$+ \frac{(m_1 + m_2 + ar)(m_1 + ar)(m_2 + ar)}{(m_1 + m_2 + 2ar)^2}\left[\arcsin v_{\perp_1} + \arcsin v_{\perp_2}\right] \ . \tag{21}$$

and the state mass M from (10) is

$$M = \sqrt{\frac{m_1 + m_2 + ar}{m_1 + m_2 + 2ar}}\left[\sqrt{m_1(m_1 + ar)} + \sqrt{m_2(m_2 + ar)}\right]$$
$$+ \frac{\sqrt{ar(m_1 + m_2 + ar)(m_1 + ar)(m_2 + ar)}}{m_1 + m_2 + 2ar}\left[\arcsin v_{\perp_1} + \arcsin v_{\perp_2}\right] \ . \tag{22}$$

In (21) and (22) $v_{\perp_1}$ and $v_{\perp_2}$ are functions of r given by (18) and (19). The above circular solutions reduce to the equal mass case considered earlier [11].

Now we can easily establish three limiting cases:

1. Heavy-heavy case ($m_1, m_2 \gg ar$)

Equations (21) and (22) can be expanded in the small quantities $\frac{ar}{m_1}$ and $\frac{ar}{m_2}$ with results

$$J^2 = \left(\frac{m_1 m_2 a}{m_1 + m_2}\right) r^3 \ , \tag{23}$$

$$M = m_1 + m_2 + \frac{3}{2}ar \ . \tag{24}$$

From the above the shifted Regge slope is

$$\frac{dJ}{d(M - m_1 - m_2)^2} = \left(\frac{m_1 m_2}{m_1 + m_2}\right)^{\frac{2}{3}} \frac{J^{-\frac{1}{3}}}{3a^{\frac{1}{3}}} \ . \tag{25}$$

2. **Heavy-light case** ($m_1 = 0, m_2 \gg ar$)

Again, from (21) and (22) in this limit we find

$$J = \frac{\pi a r^2}{4} , \tag{26}$$

$$M = m_2 + \frac{\pi a r}{2} . \tag{27}$$

Eliminating r the shifted Regge slope is

$$\frac{J}{(M - m_2)^2} = \frac{1}{\pi a} . \tag{28}$$

3. **Light-light case** ($m_1 = m_2 = 0$)

For zero mass quarks the tube carries all the rotational momentum and energy of the meson. In this limit we obtain

$$J = \frac{\pi a r^2}{8} , \tag{29}$$

$$M = \frac{\pi a r}{2} . \tag{30}$$

giving a Regge slope (Nambu) of

$$\frac{J}{M^2} = \frac{1}{2\pi a} . \tag{31}$$

The various limiting situations are illustrated in Figs. 2 and 3. We choose $m_2 = 1.5GeV$, $a = (2\pi)^{-1}GeV^2$ and plot the shifted Regge slope as a function of J. In Fig. 2 we take $m_1 = 0$. The solid curve shows a shifted slope of 2 units at small J as expected from the heavy-light limit of (28). At large J where $m_2 < ar$ the slope approaches the Nambu limit (31). For $m_1 = 0.5GeV$ the solid curve of Fig. 3 illustrates the yrast shifted Regge slope. At small J the heavy-heavy limit (25) is obtained, and for large J again the Nambu limit of unit slope is obtained. In both Figs. 2 and 3 the dashed curve is the quantum solution which will be discussed in section 4.

3 Quantization of the Classical Equations

3.1 Equal-mass and the heavy-light case

The classical equations (1-7) for the equal-mass case reduce to

$$\frac{J}{r} = W_r \gamma_\perp v_\perp + ar f(v_\perp) , \tag{32}$$

$$H = 2W_r \gamma_\perp + ar \frac{\arcsin v_\perp}{v_\perp} , \tag{33}$$

with

$$W_r = \sqrt{p_r^2 + m^2} \tag{34}$$

and

$$f(v_\perp) = \frac{1}{4v_\perp}\left(\frac{\arcsin v_\perp}{v_\perp} - \frac{1}{\gamma_\perp}\right) , \tag{35}$$

Since in the limit of large quark masses [1, 3]

$$v_{\perp i} \to \frac{J}{m_i r} , \tag{36}$$

we have a good reason to believe that $v_{\perp_1}$ and $v_{\perp_2}$ should be hermitian operators. Also, if we could invert the classical angular momentum equation for the equal-mass case (32), we would have

$$v_\perp = v_\perp(r, p_r, J) , \tag{37}$$

which means that $[v_\perp, r] \neq 0$ when $v_\perp$ and r are considered as quantum-mechanical operators. Therefore, the classical equations should be symmetrized and quantized as [1]

$$J \to \sqrt{l(l+1)}, \quad p_r^2 \to -\frac{1}{r}\frac{\partial^2}{\partial r^2} r , \tag{38}$$

$$2\frac{\sqrt{l(l+1)}}{r} = \{W_r, \gamma_\perp v_\perp\} + a\{r, f(v_\perp)\} , \tag{39}$$

$$H = \{W_r, \gamma_\perp\} + \frac{a}{2}\{r, \frac{\arcsin v_\perp}{v_\perp}\} , \tag{40}$$

where $\{A, B\} \equiv AB + BA$. Similarly, the heavy-light case classical equations with m_2 as the heavy quark mass,

$$\frac{J}{r} = W_r \gamma_\perp v_\perp + 2arf(v_\perp) , \tag{41}$$

$$H = m_2 + W_r \gamma_\perp + ar\frac{\arcsin v_\perp}{v_\perp} , \tag{42}$$

after quantization become

$$\frac{\sqrt{l(l+1)}}{r} = \frac{1}{2}\{W_r, \gamma_\perp v_\perp\} + a\{r, f(v_\perp)\} , \tag{43}$$

$$H = m_2 + \frac{1}{2}\{W_r, \gamma_\perp\} + \frac{a}{2}\{r, \frac{\arcsin v_\perp}{v_\perp}\} . \tag{44}$$

3.2 General case

In the general case with $m_1 \neq m_2$ things get more complicated. Besides equation defining the angular momentum, we also require that total momentum of the system must be zero, which is trivially satisfied in the two special cases considered above.

We begin by using the straight tube condition (8) and the quark separation variable (15) which give

$$r_i = \frac{v_{\perp_i}}{v_{\perp_1} + v_{\perp_2}} r , \qquad i = 1, 2 . \tag{45}$$

The classical RFT equations (1-7) can then be expressed in terms of $v_\perp$'s and r:

$$\frac{J}{r} = W_{r_1}\frac{\gamma_{\perp_1} v_{\perp_1}^2}{v_{\perp_1} + v_{\perp_2}} + W_{r_2}\frac{\gamma_{\perp_2} v_{\perp_2}^2}{v_{\perp_1} + v_{\perp_2}} + ar\frac{1}{(v_{\perp_1} + v_{\perp_2})^2}(\tilde{f}(v_{\perp_1}) + \tilde{f}(v_{\perp_2})) , \tag{46}$$

$$P_\perp = 0 = W_{r_1}\gamma_{\perp_1} v_{\perp_1} - W_{r_2}\gamma_{\perp_2} v_{\perp_2} - ar\frac{1}{v_{\perp_1} + v_{\perp_2}}(\frac{1}{\gamma_{\perp_1}} - \frac{1}{\gamma_{\perp_2}}) , \tag{47}$$

$$H = W_{r_1}\gamma_{\perp_1} + W_{r_2}\gamma_{\perp_2} + ar\frac{1}{v_{\perp_1} + v_{\perp_2}}(\arcsin v_{\perp_1} + \arcsin v_{\perp_2}) . \tag{48}$$

Here we have

$$W_{r_i} = \sqrt{p_r^2 + m_i^2} , \tag{49}$$

because of radial momentum conservation, and function $\tilde{f}(v_\perp)$ is defined as

$$\tilde{f}(v_\perp) = \frac{1}{2}(\arcsin v_\perp - \frac{v_\perp}{\gamma_\perp}) . \tag{50}$$

If we could invert equations (46) and (47) for $v_{\perp_1}$ and $v_{\perp_2}$, they would be in general different functions of r, p_r and J, so that corresponding quantum mechanical operators will not commute. Therefore, our quantized equations will contain products of three non-commuting factors, and we have to find the way to symmetrize them. In doing that, we have to keep in mind that our procedure must reduce to equations (39,40) and (43,44) in the equal-mass and the heavy-light limits, respectively. The easiest way to ensure this is to symmetrize first between non-commuting factors containing $v_{\perp_1}$ and $v_{\perp_2}$ to obtain symmetric operators $\hat{\mathcal{O}}(v_{\perp_1}, v_{\perp_2})$, and then to symmetrize between these operators and radial operators. If we do that, our quantized equations (46-48) become

$$\frac{\sqrt{l(l+1)}}{r} = \frac{1}{2}\{W_{r_1}, \frac{1}{2}\{\gamma_{\perp_1} v_{\perp_1}^2, \frac{1}{v_{\perp_1} + v_{\perp_2}}\}\} + \frac{1}{2}\{W_{r_2}, \frac{1}{2}\{\gamma_{\perp_2} v_{\perp_2}^2, \frac{1}{v_{\perp_1} + v_{\perp_2}}\}\} + \frac{1}{2}a\{r, \frac{1}{2}\{\tilde{f}(v_{\perp_1}) + \tilde{f}(v_{\perp_2}), \frac{1}{(v_{\perp_1} + v_{\perp_2})^2}\}\} , \tag{51}$$

$$P_\perp = 0 = \frac{1}{2}\{W_{r_1}, \gamma_{\perp_1} v_{\perp_1}\} - \frac{1}{2}\{W_{r_2}, \gamma_{\perp_2} v_{\perp_2}\} - \frac{a}{2}\{r, \frac{1}{2}\{\frac{1}{v_{\perp_1} + v_{\perp_2}}, \frac{1}{\gamma_{\perp_1}} - \frac{1}{\gamma_{\perp_2}}\}\} , \tag{52}$$

$$H = \frac{1}{2}\{W_{r_1}, \gamma_{\perp_1}\} + \frac{1}{2}\{W_{r_2}, \gamma_{\perp_2}\} + \frac{a}{2}\{r, \frac{1}{2}\{\frac{1}{v_{\perp_1} + v_{\perp_2}}, \arcsin v_{\perp_1} + \arcsin v_{\perp_2}\}\} . \quad (53)$$

4 Numerical Solution of the Quantized Equations

The RFT hamiltonian (53) contains two unknown operators, $v_{\perp_1}$ and $v_{\perp_2}$, which are in turn defined by equations (51) and (52). If we introduce a complete set of basis states $\{e_k(\mathbf{r})\}$ and then truncate at a finite number N [12],

$$\psi(\mathbf{r}) \simeq \sum_{k=1}^{N} c_k e_k(\mathbf{r}) , \quad (54)$$

these equations become two coupled transcendental $N \times N$ matrix equations involving unknown matrices of $v_{\perp_1}$ and $v_{\perp_2}$, and known r, $\frac{1}{r}$, and W_{r_i} matrices [4]. Our numerical solution for $v_{\perp_1}$ and $v_{\perp_2}$ is based on a simple $x = F(x)$ iteration algorithm applied to transcedental matrix equations.

Equation (51) can be written in the form

$$W_{r_1}\frac{1}{v_{\perp_1} + v_{\perp_2}}\gamma_{\perp_1}v_{\perp_1}^2 = 4\frac{\sqrt{l(l+1)}}{r} - W_{r_1}\gamma_{\perp_1}v_{\perp_1}^2\frac{1}{v_{\perp_1} + v_{\perp_2}} - \{\gamma_{\perp_1}v_{\perp_1}^2, \frac{1}{v_{\perp_1} + v_{\perp_2}}\}W_{r_1} - \{W_{r_2}, \{\gamma_{\perp_2}v_{\perp_2}^2, \frac{1}{v_{\perp_1} + v_{\perp_2}}\}\} - a\{r, \{\tilde{f}(v_{\perp_1}) + \tilde{f}(v_{\perp_2}), \frac{1}{(v_{\perp_1} + v_{\perp_2})^2}\}\} . \quad (55)$$

If we multiply this equation by $v_{\perp_1}^{-1}\gamma_{\perp_1}^{-1}(v_{\perp_1} + v_{\perp_2})W_{r_1}^{-1}$ from the left, we get

$$v_{\perp_1} = v_{\perp_1}^{-1}\gamma_{\perp_1}^{-1}(v_{\perp_1} + v_{\perp_2})W_{r_1}^{-1}\ (4\frac{\sqrt{l(l+1)}}{r} - W_{r_1}\gamma_{\perp_1}v_{\perp_1}^2\frac{1}{v_{\perp_1} + v_{\perp_2}}$$

$$- \{\gamma_{\perp_1}v_{\perp_1}^2, \frac{1}{v_{\perp_1} + v_{\perp_2}}\}W_{r_1} - \{W_{r_2}, \{\gamma_{\perp_2}v_{\perp_2}^2, \frac{1}{v_{\perp_1} + v_{\perp_2}}\}\} - a\{r, \{\tilde{f}(v_{\perp_1}) + \tilde{f}(v_{\perp_2}), \frac{1}{(v_{\perp_1} + v_{\perp_2})^2}\}\}\ ) . \quad (56)$$

We can do the same thing with equation (52) and obtain

$$v_{\perp_1} = \gamma_{\perp_1}^{-1}W_{r_1}^{-1}\ (-\gamma_{\perp_1}v_{\perp_1}W_{r_1} + \{W_{r_2}, \gamma_{\perp_2}v_{\perp_2}\} + a\{r, \frac{1}{2}\{\frac{1}{v_{\perp_1} + v_{\perp_2}}, \frac{1}{\gamma_{\perp_1}} - \frac{1}{\gamma_{\perp_2}}\}\}\ ) . \quad (57)$$

For a succesful itterative solution we must start with a good initial guess for matrices of $v_{\perp_1}$ and $v_{\perp_2}$. We then have an initial guesses for matrices of all functions of these two operators and we can evaluate the right sides of equations (56) and (57) as the new guesses for $v_{\perp_1}$ matrix (let us call them $v_{\perp_1}(J)$ and $v_{\perp_1}(P_\perp)$. Since we want to have both equations (51) and (52) satisfied simultaneously, we mix these two guesses with weights depending on the extent to which the equations (51) and (52) are satisfied, with the initial guesses for $v_{\perp_1}$ and $v_{\perp_2}$. For example, if the equation (51) is satisfied twice as well as the equation (52), then for the new guess for $v_{\perp_1}$ we take $\frac{1}{3}v_{\perp_1}(J) + \frac{2}{3}v_{\perp_1}(P_\perp))$. This ensures that both equations defining $v_{\perp_1}$ and $v_{\perp_2}$ will be simultaneously satisfied. Finally, since we are solving for matrices here, it is clear that our iteration scheme will be only marginally stable, and for that reason we have to change $v_{\perp_i}$ matrices very slowly. Therefore, for the final new guess for $v_{\perp_1}$ we take $(1-\eta)v_{\perp_1}(old) + \eta v_{\perp_1}(new)$, where η is the small number (usually $\eta \leq 0.1$, and it becomes smaller if we increase number N of the basis states that we are working with). After we have found the new guess for $v_{\perp_1}$, we do the same thing for $v_{\perp_2}$, and keep iterating until we achieve the required precision.

Using the same procedure, we were able to solve for $v_\perp$ the equal-mass and the heavy-light case equations (39,43) even for as many as 50 basis states without too much effort and to a very high accuracy of 8 decimal places. The initial guess in

these two cases we can obtain by finding the $v_\perp$ from the non-symmetrized angular momentum equations [4], and then symmetrizing it by taking the average of the non-symmetric $v_\perp$ matrix and its transpose. The eigenvalues obtained from the symmetrized hamiltonians (40,44) are usually a couple of MeV's lower than the eigenvalues obtained from the non-symmetrized equations. In Fig.4 we compare the non-symmetrized solution [4] for $m_1 = m_2 = 0$ (solid curve) with the symmetrized solution shown at integral angular momentum quantum number l. The difference between symmetrized and unsymmetrized solution is at most a couple of MeV's over a wide range of rotational and radial excited states. With increase of quark masses this difference decreases.

In the general case we have two unknown matrices and the equations are much more complicated. In addition, a good initial guess for $v_{\perp_1}$ and $v_{\perp_2}$ is not easy to find. Usually, for the initial guess for $v_{\perp_i}$ in the case of $l > 0$ (for $l = 0$ solution is trivial, $v_{\perp_1} = v_{\perp_2} = 0$) we use symmetrized equal-mass guess for $m = m_i$ and the same angular momentum quantum number l. Despite these complications, for $N \leq 10$ basis states we have found that our procedure converges very quickly no matter how large the difference between m_2 and m_1 is (i.e., no matter how bad initial guess is). In comparing with experimental data, we require only the lowest one or two eigenvalues, and these are determined within 10 MeV if we use 5, and within 1 MeV if we use 10 basis states. Fits with $N = 10$ are reliable and completely adequate for our purposes.

In Figs. 2 and 3 we compare the ground state quantum solution (for continuous values of l [4]) with the classical yrast solution. We show in these figures the predicted shifted Regge slope. The correspondence limit at large angular momentum is well satisfied.

5 Comparison with Experiment

As mentioned earlier, mesons containing at least one heavy quark will have relatively small dependances on quark spins. It seems realistic then to compare our predictions, which do not include quark spin, directly to spin averaged energy levels. There are however two additions to the model which must be incorporated in order to have a phenomenologically successful result.

5.1 Short range interaction

The flux tube configuration has been assumed to dominate when the quarks are widely separated. At short distance there must be an attractive singular interaction due to the single gluon exchange. We parametrize short and intermediate distance interaction by the usual potential

$$V_S(r) = -\frac{\kappa}{r} , \tag{58}$$

where at short distances $\kappa = \frac{4}{3}\alpha_s$. In the static limit the total potential then reduces to the well known "Cornell potential" [13]: a superposition of linear confinement $V_{conf} = ar$ and the Coulombic term (58). From general consideration we expect κ to "run" such that it will increase slowly as the quarks are separated. In our comparison with data we will allow different κ's for heavy-heavy and heavy-light mesons.

5.2 Constant term

A constant term is also added to the hamiltonian giving

$$H = H_{RFT} + C - \frac{\kappa}{r} , \tag{59}$$

with H_{RFT} given by (53). Just as the dynamical Wilson loop "area term" generates precisely the RFT equations of motion [14], the Wilson loop "perimeter term" adds

a constant C to the static potential [6]. For heavy quarks it has been shown [6] that, up to order $\frac{1}{m^2}$ in the heavy quark mass, the constant C just renormalizes the quark mass.

$$m_i \to m_i + \frac{1}{2}C \ . \tag{60}$$

This is not quite the case for light quarks as we shall show. It has been further suggested [15] that there is a fundamental relationship between the constant term in the potential and the string tension a,

$$C = -2e^{\frac{1}{2}-\gamma}\sqrt{a} \simeq -2\sqrt{a} \simeq -800MeV \ , \tag{61}$$

where $\gamma = 0.57712\ldots$ is the Euler constant.

5.3 The Data and Comparison with Theory

We have used the quark model spectroscopic assigments and level masses of the *Particle Data Group* [16] to extract spin averaged states for heavy-light mesons (Table 1) and heavy-heavy mesons below flavor treshold (Table 2). To account for these spin averged levels we must choose the quark masses $m_{u,d}$, m_s, m_c and m_b, and the interaction parameters κ_{HL}, κ_{HH}, a, and C properly. We see from (60) that the additive constant C will be strongly correlated with the quark masses. In fact we find that a family of nearly equivalent solutions occur for a range of negative values of C. In our fit to the data of Tables 1 and 2 we fix $m_{u,d}$ and vary all the other quark masses, the tension a, the constant term C, and the short-range potential constants κ_{HL} and κ_{HH} for heavy-light and heavy-heavy mesons, respectively. Essentially equivalent fits to the data are found over a wide range of $m_{u,d}$ values. In Figure 5 we show explicitly the correlation between the light quark mass $m_{u,d}$ and C. In Figs. 6 and 7 we show the correlation of the other interaction parameters on the choice of $m_{u,d}$. We note from Fig. 7 that κ_{HH} is only slightly dependent on $m_{u,d}$ (or equivalently on C). This is to be expected since the QCD heavy quark mass scaling

relation (60) becomes exact for two heavy quarks. From Fig. 7 we also see that the heavy-light short range constant κ_{HL} is larger than κ_{HH} only for $m_{u,d}$ smaller than $400MeV$. Since the heavy-light mesons are spatially larger than the heavy-heavy mesons, one should expect that κ_{HL} should exceed κ_{HH} on the general QCD grounds. Accepting this argument then indicates a preference for the light quark constituent mass. The usual $m_{u,d} \simeq 300MeV$ is quite acceptable. By the same argument using Fig. 5 the less negative values of C are indicated. In particular, the Gromes value (61) would seem to be too negative. In Figs. 8 to 10 we show the dependence of the fitted heavier quark masses on the choice of $m_{u,d}$ (or equivalently C). The charm and bottom clearly satisfy the QCD scaling relation (60). For the choice of $m_{u,d} = 300MeV$ the values of the fitted parameters are

$$\begin{aligned} a &= 0.20GeV^2 \ , \\ \kappa_{HH} &= 0.45 \ , \\ \kappa_{HL} &= 0.46 \ , \\ C &= -580MeV \ , \\ m_s &= 480MeV \ , \\ m_c &= 1655MeV \ , \\ m_b &= 5040MeV \ . \end{aligned} \tag{62}$$

The fitted values for the spin-averaged meson masses are given in Tables 1 and 2, respectively. The resulting masses generally agree with the data to better than 20 or 30 MeV.

6 Conclusions

In this paper we have discussed the relativistic flux tube model with arbitrary mass spinless quarks on the ends of the flux tube. We have obtained the classical rotational

solution (yrast). The quantum solution is also proposed and solved numerically. We have confined our comparison of the RFT with data to mesons containing at least one heavy quark primarily because in this case spin dependence should be small enough that the spin averaged data can be compared to our spinless quark calculation. We have done a simultaneous fit to all of the available heavy-light and heavy-heavy data. We find that the same parameters which arise in the usual heavy onia analyses [12] apply to the heavy-light states as well. The one main difference is that a constant term now must be added to the hamiltonian (59). When only heavy onia were considered an additive constant was arbitrary due to the QCD scaling relation (60). With the addition of heavy-light mesons, the constant C still can vary quite a bit, but $C = 0$ for example is excluded.

From Fig. 11 we observe that difference in quark masses are much better defined than the individual quark masses. In particular, we have

$$m_b - m_c = 3385 \pm 20 MeV \ . \tag{63}$$

Upon closer inspection of the fit in Table 1 we see that for heavy-light mesons those containing a charm quark are overestimated by $25 MeV$, while those containing a bottom quark are underestimated by about $20 MeV$. This indicates that the heavy quark difference $m_b - m_c$ should be about 45 MeV smaller for heavy-light mesons than the one for heavy-heavy mesons. This discrepancy was pointed out some time ago [17] and still persists even in the context of a more sophisticated treatment.

It will be important to include spin in our model. Fortunately the orbital angular momentum discussion in this paper will form a key ingredient of the more complete calculation. The results will be somewhat different even for the spin averaged case since a Darwin type term will arise due to the fermionic nature of the quarks both at long and short range. The RFT model formulation with fermionic quarks has been discussed in some detail [3] previously.

ACKNOWLEDGMENTS

We would like to thank Collin Olson for helpful discussions. This work was supported in part by the U.S. Department of Energy under Contract No. DE-AC02-76ER00881 and in part by the University of Wisconsin Research Commitee with funds granted by the Wisconsin Alumni Research Foundation.

References

[1] Dan LaCourse and M. G. Olsson, Phys. Rev. D **39**, 2751 (1989).

[2] Collin Olson, M. G. Olsson and Ken Williams, Phys. Rev. D **45**, 4307 (1992).

[3] M. G. Olsson and Ken Williams, Phys. Rev. D **48**, 417 (1993).

[4] C. Olson, M. G. Olsson and D. LaCourse, *The Quantized Relativistic Flux Tube*, UW-Madison preprint MAD/PH/761, to be published in Phys. Rev. D.

[5] E. Eichten and F. Feinberg, Phys. Rev. D **23**, 2724 (1981); D. Gromes, Z. Phys. C **22**, 265 (1984); **26**, 401 (1984); A. Barchielli, E. Montaldi and G. M. Prosperi, Nucl. Phys. **B296**, 625 (1988); **B303**, 752(E) (1988).

[6] A. Barchielli, N. Brambilla and G. M. Prosperi, Nuovo Cim **103A**, 59 (1989).

[7] N. Brambilla and G. M. Prosperi, Phys. Lett. **236B**, 69 (1990).

[8] W. Buchmüller, Phys. Lett. **112B**, 479 (1982).

[9] Robert D. Pisarski and John D. Stack, Nucl. Phys. **286B**, 657 (1987).

[10] E. E. Salpeter, Phys. Rev. **87**, 328 (1952).

[11] Alan Chodos and Charles B. Thorn, Nucl. Phys. **B72**, 509 (1974); M. Ida, Prog. Theor. Phys. **59**, 1661 (1978).

[12] A discussion of the Galerkin method and the definition of the specific basis states used here is found in S. Jacobs, M. G. Olsson and C. J. Suchyta III, Phys. Rev. D **33**, 3338 (1986).

[13] T. Appelquist, R. M. Barnett and K. D. Lane, Ann. Rev. Nuc. Part. Sci. **28**, 38 (1978).

[14] A. Yu. Dubin, A. B. Kaidalov and Yu. A. Simonov, Yadernaya Fizika **56**, 12 (1993), in press.

[15] D. Gromes, Z. Phys. C **11**, 147 (1981).

[16] Particle Data Group, Phys. Rev. D **45**, 51 (1992); F. Abe et al. (CDF Collaboration), Fermilab-Pub-93/141-E; D. Buskulic et al. (ALEPH Collaboration), CERN-PPE/93-97; P. D. Acton et al. (OPAL Collaboration), Phys. Rev. Lett. B **295**, 357 (1992).

[17] M. G. Olsson, Phys. Lett. **139B**, 417 (1984).

TABLES

Table 1: Heavy-light spin averaged states. Spin-averaged masses are calculated in the usual way, by taking $\frac{3}{4}$ of the triplet and $\frac{1}{4}$ of the singlet mass.

state	spectroscopic label J^P	spectroscopic label $^{2S+1}L_J$	spin-averaged mass (MeV)	theory (MeV)	error (MeV)
$c\bar{u}$, $c\bar{d}$ quarks					
D (1867)	0^-	$^1S_0$	$1S$ (1974)	2000	26
D^* (2009)	1^-	$^3S_1$			
D_1 (2424)	1^+	$^1P_1$	$1P$ (2424)	2419	−5
$c\bar{s}$ quarks					
D_s (1969)	0^-	$^1S_0$	$1S$ (2075)	2105	30
D_s^* (2110)	1^-	$^3S_1$			
D_{s_1} (2537)	1^+	$^1P_1$	$1P$ (2537)	2526	−11
$b\bar{u}$, $b\bar{d}$ quarks					
B (5279)	0^-	$^1S_0$	$1S$ (5312)	5293	−19
B^* (5325)	1^-	$^3S_1$			
$b\bar{s}$ quarks					
B_s (5368)	0^-	$^1S_0$	$1S$ (5409)	5389	−20

Table 2: Heavy-heavy spin averaged states. Since η_b's have not been observed yet, in calculating spin averaged mass for all S states in $b\bar{b}$ system we assume $\Upsilon - \eta_b = 40 \pm 20 MeV$ on the grounds that this splitting should be approximately one third of the corresponding splitting in the $c\bar{c}$ systems. We estimate that the error introduced in this way is probably less than $5 MeV$. We also assume that p-wave hyperfine splitting in the $b\bar{b}$ mesons is negligible.

state	spectroscopic label J^P	spectroscopic label $^{2S+1}L_J$	spin-averaged mass (MeV)	theory (MeV)	error (MeV)
$c\bar{c}$ quarks					
η_c (2979)	0^-	$^1S_0$	$1S$ (3068)	3077	9
ψ (3097)	1^-	$^3S_1$			
χ_{0c} (3415)	0^+	$^3P_0$	$1P$ (3525)	3494	−31
χ_{1c} (3511)	1^+	$^3P_1$			
χ_{2c} (3556)	2^+	$^3P_2$			
h_c (3525)	1^+	$^1P_1$			
η_c' (3594)	0^-	2^1S_0	$2S$ (3663)	3665	2
ψ' (3686)	1^-	2^3S_1			
$b\bar{b}$ quarks					
Υ (9460)	1^-	$^3S_1$	$1S$ (9450)	9444	−6
Υ' (10023)	1^-	2^3S_1	$2S$ (10013)	10009	−4
Υ'' (10355)	1^-	3^3S_1	$3S$ (10345)	10360	15
χ_{0b} (9860)	0^+	$^3P_0$	$1P$ (9900)	9908	8
χ_{1b} (9892)	1^+	$^3P_1$			
χ_{2b} (9913)	2^+	$^3P_2$			
χ_{0b}' (10232)	0^+	2^3P_0	$2P$ (10261)	10268	7
χ_{1b}' (10255)	1^+	2^3P_1			
χ_{2b}' (10268)	2^+	2^3P_2			

FIGURES

Figure 1: Portion of a meson consisting of a segment of flux tube from the center of momentum to the i^{th} quark.

Figure 2: Yrast solution (solid curve) compared to the quantum solution (dashed curve) for $m_1 = 0$ and $m_2 = 1.5GeV$. We compare our solution for the same value of J (yrast) and l (quantum).

Figure 3: Yrast solution (solid curve) compared to the quantum solution (dashed curve) for $m_1 = 0.5GeV$ and $m_2 = 1.5GeV$.

Figure 4: Comparison of the symmetrized and non-symmetrized equations for quark masses $m_1 = m_2 = 0$ and $N = 50$ basis states. The non-symmetrized equations (32) and (33) discussed in [4] are found to agree with the fully symmetrized solutions of (39) and (40) to better than $5MeV$.

Figure 5: Dependence of C on $m_{u,d}$. Nearly equivalent solutions fitting the data of Tables 1 and 2 are found for the range of $m_{u,d}$ shown.

Figure 6: Dependence of a on $m_{u,d}$. The string tension is nearly independent of the choice of $m_{u,d}$.

Figure 7: Comparison of κ_{HL} and κ_{HH}. To realize the normal QCD running of κ we must take $m_{u,d}$ less than $0.4GeV$.

Figure 8: Dependence of m_s on $m_{u,d}$. The strange quark mass does not quite scale according to the QCD scaling relation (60) valid for the heavy quarks.

Figure 9: Dependence of m_c on $m_{u,d}$. The charm quark mass nearly obeys the QCD scaling relation (60).

Figure 10: Dependence of m_b on $m_{u,d}$. The bottom quark mass accurately obeys the QCD scaling relation (60).

Figure 11: Comparison of m_b, m_c, m_s. We observe that difference in quark masses are nearly independent of $m_{u,d}$ (or equivalently C).

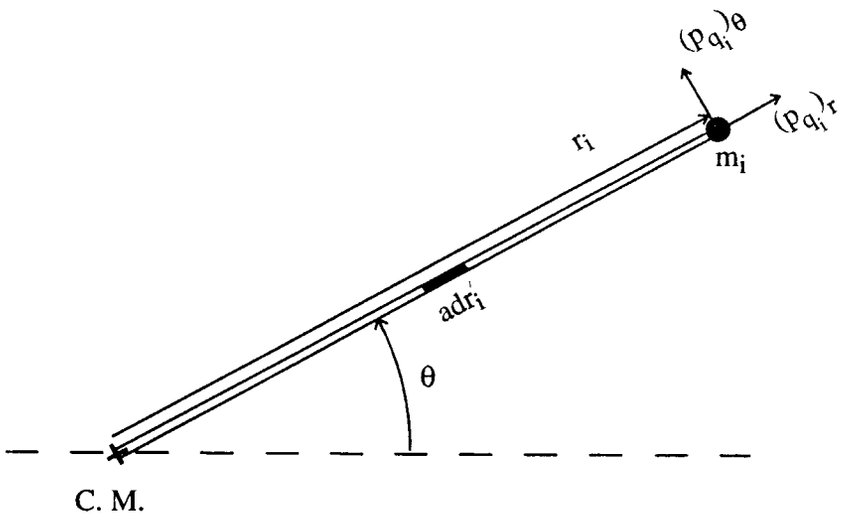

Figure 1

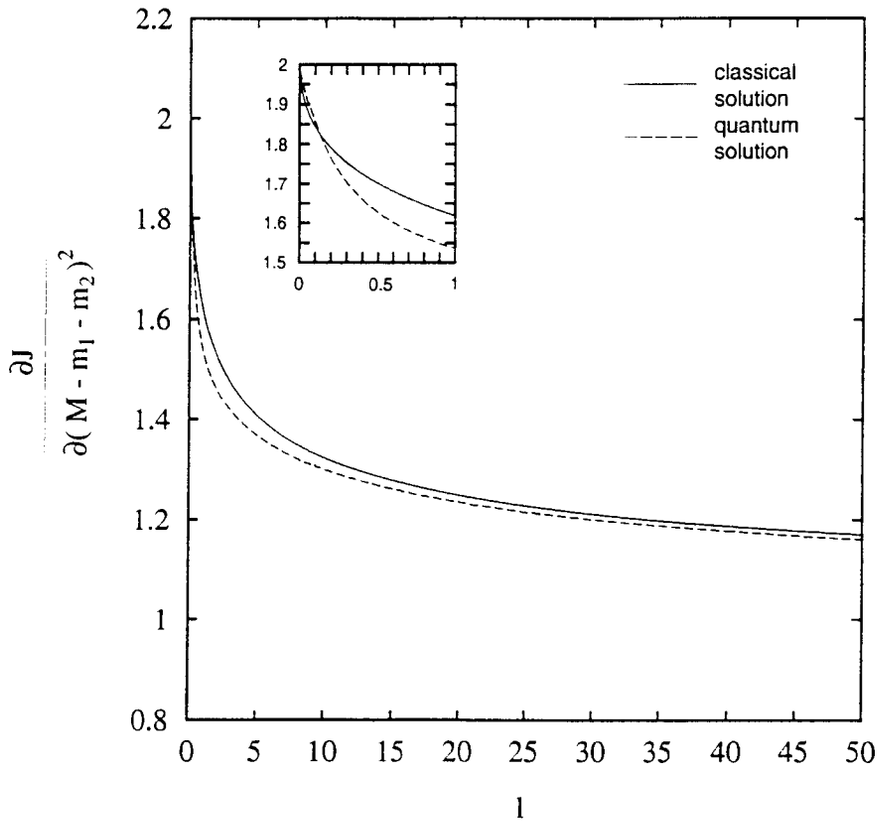

Figure 2

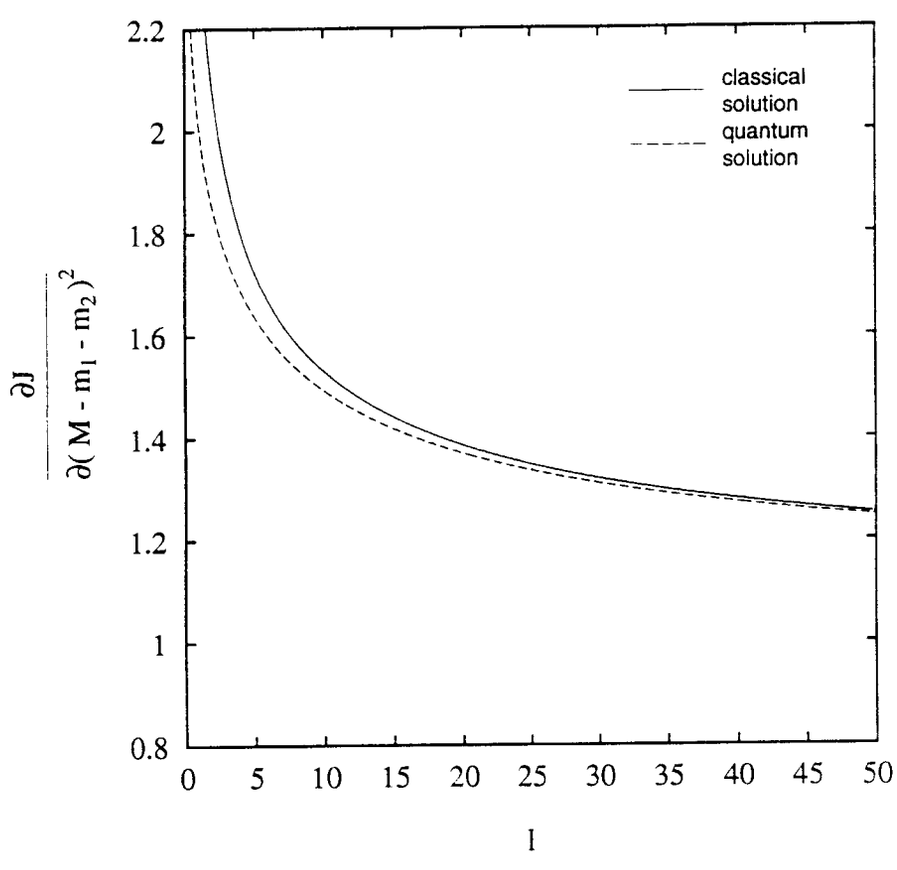

Figure 3

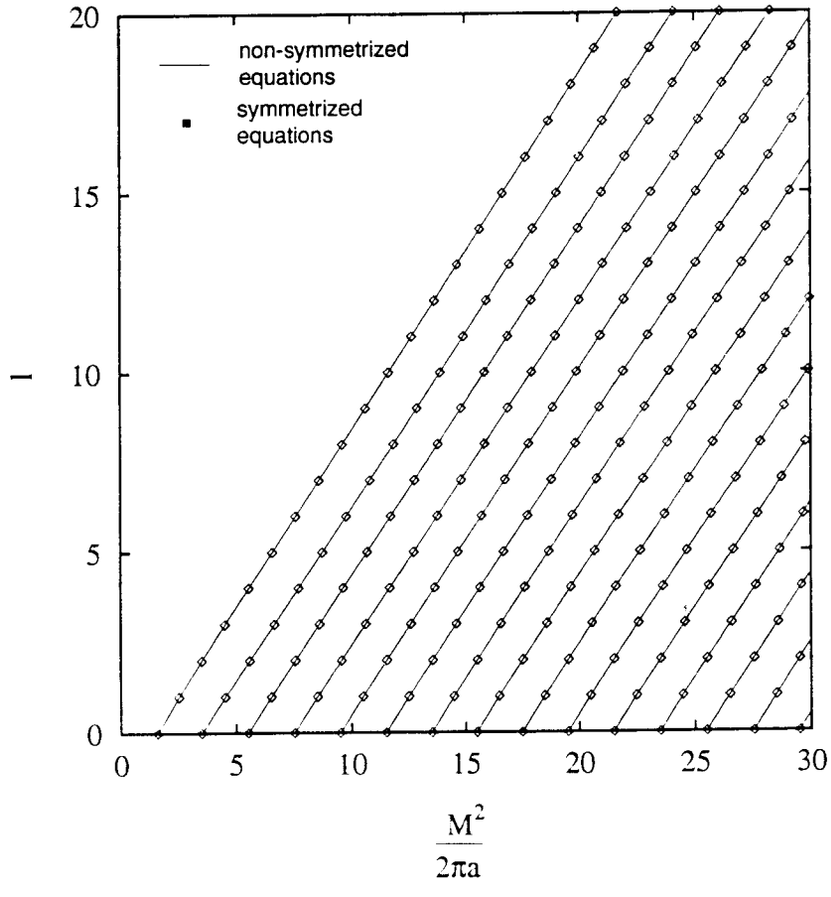

Figure 4

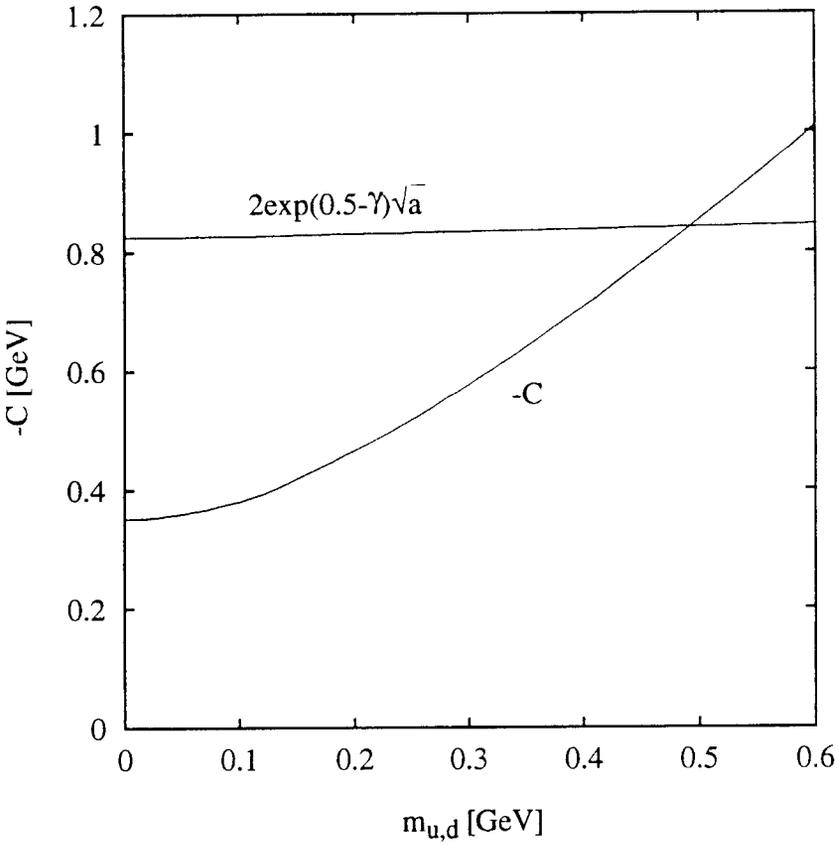

Figure 5

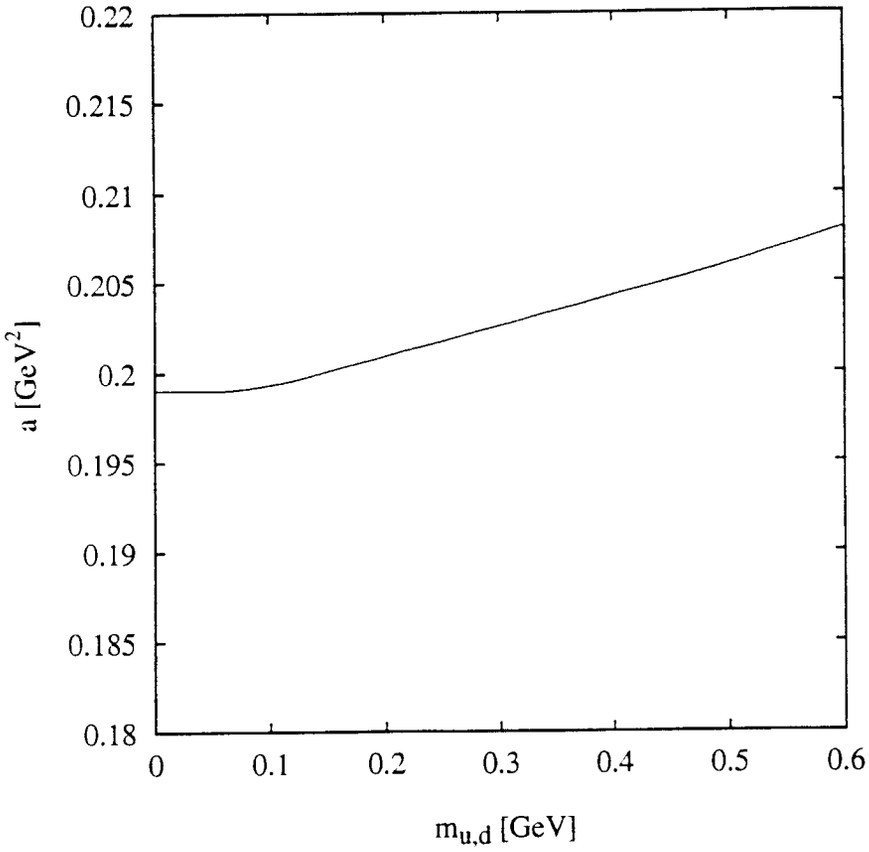

Figure 6

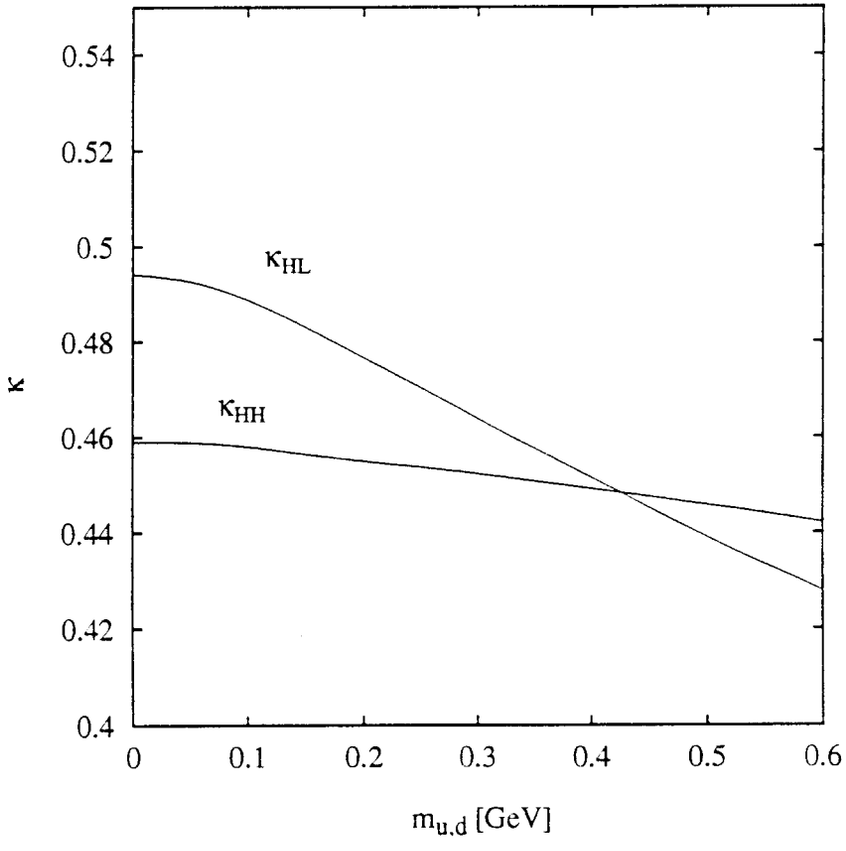

Figure 7

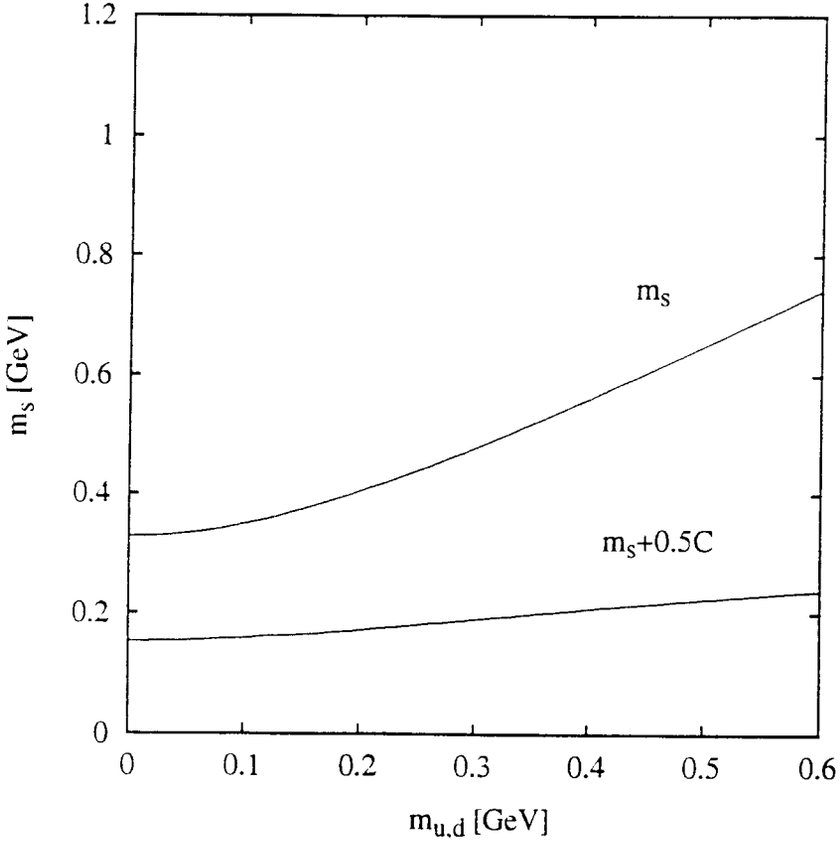

Figure 8

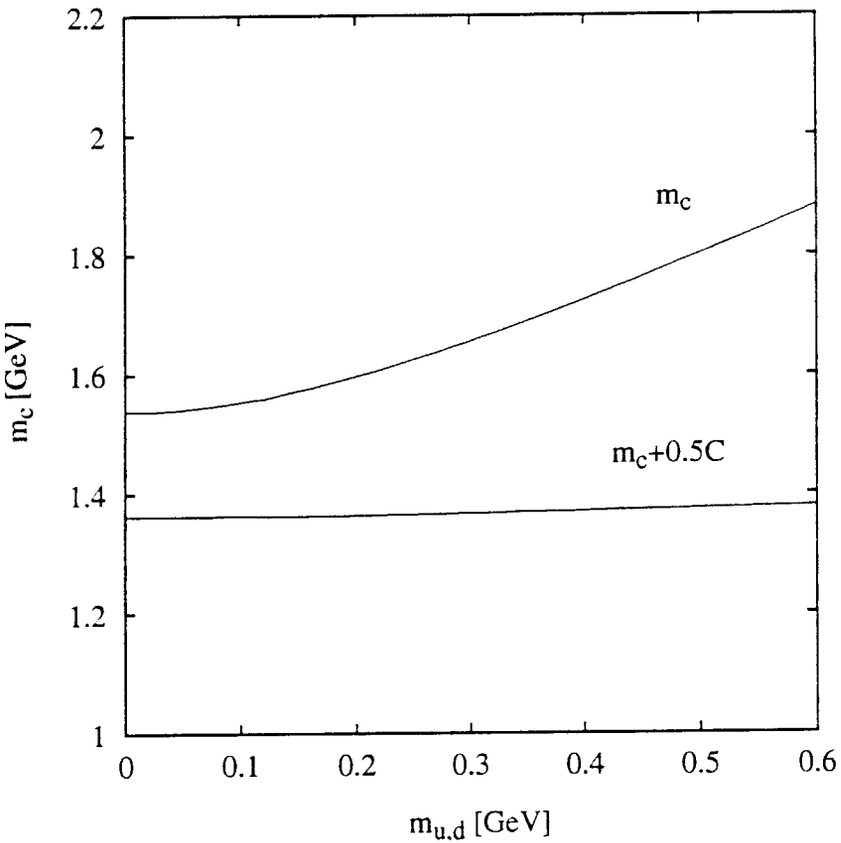

Figure 9

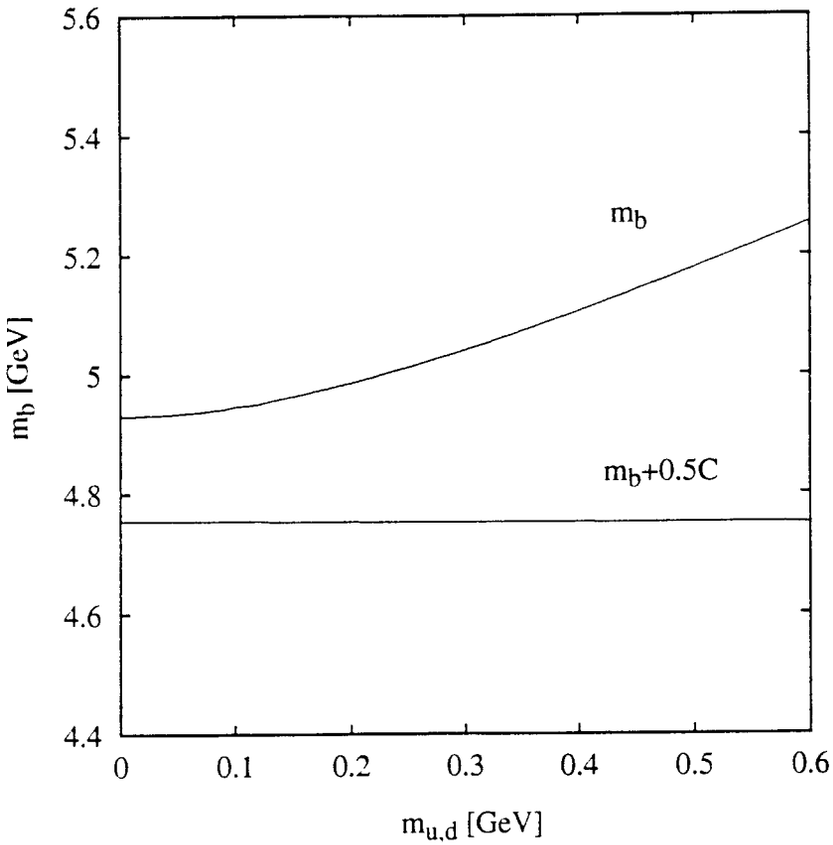

Figure 10

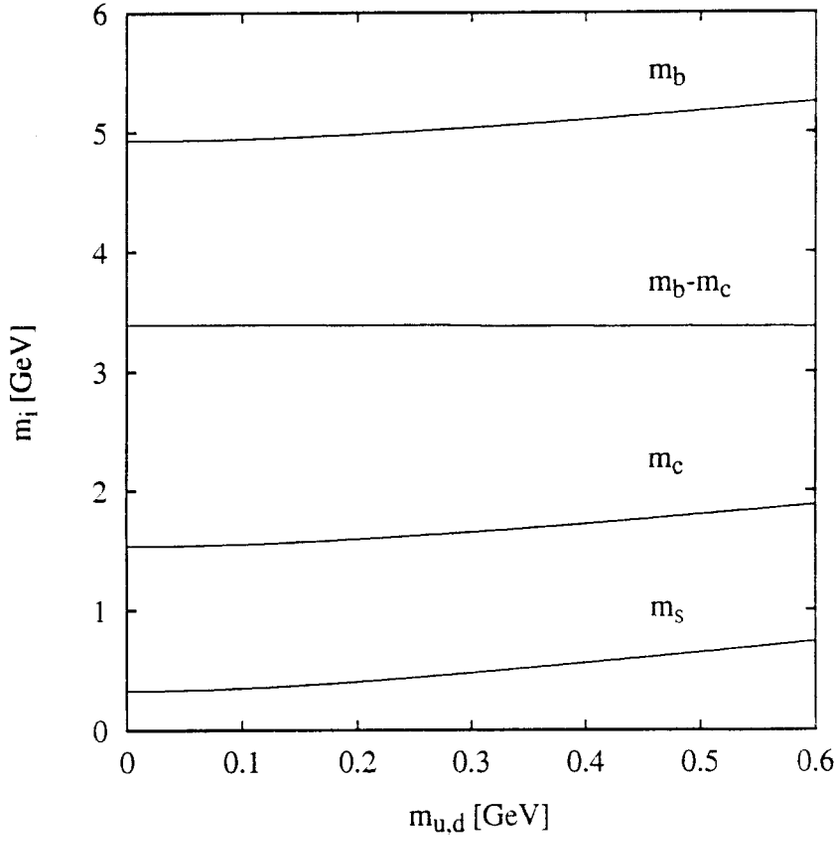

Figure 11